Battery charge and health state monitoring via ultrasonic guided-wave-based methods using built-in piezoelectric transducers

Purim Ladpli, Fotis Kopsaftopoulos, Raphael Nardari, and Fu-Kuo Chang
Department of Aeronautics and Astronautics, Stanford University, Stanford CA 94305, USA

ABSTRACT

This work presents a novel scalable and field-deployable framework for monitoring lithium-ion (Li-ion) battery state of charge (SoC) and state of health (SoH), based on ultrasonic guided waves using low-profile built-in piezoelectric transducers. The feasibility of this technique is demonstrated through experiments using surface-mounted piezoelectric disc transducers on commercial Li-ion pouch batteries. Pitch-catch guided-wave propagation is performed in synchronization with electrical charge and discharge cycling, and cycle life testing. Simple time-domain analysis shows strong and repeatable correlation between waveform signal parameters, and battery SoC and SoH. The correlation thus provides a building block for constructing a technique for accurate real-time monitoring of battery charge and health states using ultrasonic guided-wave signals. Moreover, capacity-differential signal analysis reveals the underlying physical changes associated with cyclic electrochemical activities and phase transitioning. This finding allows accurate pinpointing of the root cause of capacity fade and mechanical degradation. The results of this study indicate that the use of guided waves can potentially offer a new avenue for in-situ characterization of Li-ion batteries, providing insight on the complex coupling between electrochemistry and mechanics, heretofore not fully understood within the scientific community.

Keywords: battery management system, ultrasonic guided waves, piezoelectric transducers, lithium-ion batteries, state of charge, state of health, phase transitions, battery aging

1. INTRODUCTION

Extensive research effort in energy storage, particularly in lithium-ion (Li-ion) batteries, has been ongoing in response to the ever-growing demand for high-energy light-weight energy solutions for portable devices, and in electric systems and transportation [1-3]. Yet, their broader practical adoption has been hindered by the system's reliability, lifetime, safety, and cost. The complexity of Li-ion batteries and their narrow operational envelope require accurate real-time state monitoring for effective control and management.

Conventional on-board battery management systems (BMS) are currently limited to the monitoring of extrinsic parameters including voltage, current, and temperature. From these, battery's state of charge (SoC) and state of health (SoH) are merely approximated using state-estimation software and algorithms [4-6]. The current techniques have not yet come to exploit the fact that a Li-ion battery fundamentally is a composite material system that undergoes mechanical and chemical evolution as it cycles and ages.

In a laboratory, in-situ techniques, for instance X-ray diffraction [7-9] and neutron imaging [10, 11], can be used to effectively probe these physical changes. However, such techniques cannot be practically implemented, and in most cases can only be performed on small-scale non-standard cells. The benefits of having elaborate electrochemical tools, for instance electrochemical impedance spectroscopy (EIS) [12, 13], on-board an electric vehicle do not justify the significant additional cost and complexity.

Trying to address the aforementioned challenges, in this paper *a novel scalable and field-deployable technique for Li-ion battery SoC and SoH monitoring with ultrasonic guided waves, using minimal-footprint built-in piezoelectric wafer transducers, is introduced*. The mechanical wave propagation through the battery medium is found to accurately reflect the changes in mechanical properties as the batteries charge, discharge, and age. Analysis of the experimental guided-wave signals shows strong correlation between signal parameters, SoC and SoH, suggesting the technique can be used to

Smart Materials and Nondestructive Evaluation for Energy Systems 2017,
edited by Norbert G. Meyendorf, Proc. of SPIE Vol. 10171, 1017108
 · doi: 10.1117/12.2260107

effectively determine the battery states in a practical setting. Waveform features also demonstrate battery's phase transitioning and intercalation-induced physical changes, opening a new perspective for in-situ characterization of Li-ion batteries and electrochemical systems.

To our best knowledge, there have been similar efforts attempting using ultrasonic measurements for probing Li-ion batteries [14-16]. However, these studies are based on through-thickness transmitted and reflected bulk waves, which usually need external bulky ultrasonic probes and equipment, require extensive operator intervention, and suffer from inaccurate baseline collection. Additionally, in the study by Sood et al., only detrimental delamination of electrodes is detected – no attempt is made to quantify the non-catastrophic aging progression [14]. Gold et al. show a rough trend of signal parameters on Li-ion cells during charging and discharging [15], while a comprehensive study by Hsieh et al. does not accurately capture the gradual evolution of signals from aging [16].

The rest of this paper is structured to present the following, in respective order: method of approach, experimental setup and procedure, and experimental results. The discussion will be made alongside the results, showing our contributions which include:

- Establishment of the correlation between Li-ion battery's SoC with guided-wave signal parameters.
- Illustration of the phase transitioning and mechanical evolution through capacity-derivative analysis.
- Demonstration of SoH monitoring via tracing the aging-induced progression of signals.
- Identification of the root cause of capacity fade and mechanical degradation with guided-waves.

2. PROBLEM STATEMENT AND METHOD OF APPROACH

Prediction of SoC and particularly SoH is a challenging task for Li-ion battery system integration, with implications on accuracy, robustness, expensive computation, and cost. On-field applications are often limited to rudimentary voltage measurements and software-based prediction algorithms because the benefits of having standard laboratory equipment and electrochemical tools on board do not justify the cost and complexity. Hence it is imperative to develop an online, scalable, minimal-footprint technique to probe battery's state in service.

Therefore, this work conducts a feasibility study of using mechanical guided-wave propagation for probing and correlating the evolution of mechanical phenomena with battery's SoC and SoH. An experimental study is performed on as-received commercial Li-ion pouch batteries with surface-mounted piezoelectric transducers (Figure 1). The guided waves interact with the propagation battery medium, allowing the progression of the medium's physical properties to be interrogated during charging, discharging, and aging. Signal analysis is then performed to reveal correlation with SoC and SoH and provide a framework for a real-time on-demand battery state monitoring.

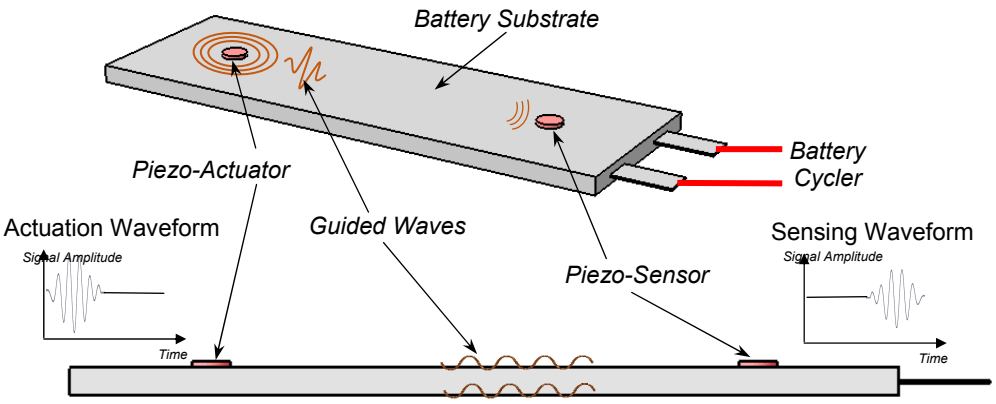

Figure 1 Schematics of ultrasonic guided-wave propagation in Li-ion battery substrate, using surface-mounted low-profile piezoelectric transducers.

3. EXPERIMENTATION

Experiments are performed on commercial Li-ion pouch batteries, with graphite/nickel-manganese-cobalt oxide (NMC) chemistry. The fresh batteries have a nominal capacity of 3650 mAh (135 x 45 x 5 mm), and are tested as received from manufacturer after a standard formation protocol. Four 6.35mm-diameter disc piezoelectric transducers (PZT-5A) in the SMART Layer format (Acellent Technologies, Inc.) are attached on the surface of the batteries using Hysol E20HP structural epoxy adhesive, according to the schematics shown in Figure 2b.

The ultrasonic data acquisition is synchronized with an eight-channel battery analyzer (BST8-3, MTI Corporation). The electrical cycling is performed with the batteries at a constant temperature in a low-temperature gravity-convection oven (Figure 2a). The piezoelectric transducers are actuated and sensed with standard five-peak Hanning-windowed tone bursts, using a 64-channel ultrasonic data acquisition system (ScanGenie II model; Acellent Technologies, Inc.). The peak-to-peak amplitude of the actuation signals is 75V. The center frequencies of the signals span between 100 to 200 kHz and are selected so as to obtain clear wave packets in the sensor response. The ultrasonic measurements are taken every 1 minute during electrical charge discharge cycles.

Guided-wave signals are collected in a pitch-catch mode whereby one transducer acts as an actuator and the others sense the incoming waves, resulting in a representative actuator-sensor response shown in Figure 3. In this work, only the time-domain analysis of the signals is presented. Figure 3 shows the two time-domain parameters of interest: the (sensing) signal amplitude, which is the maximum amplitude of the sensing signal's Hilbert envelope, and the time of flight (ToF), which is the measure of the time taken by an actuation wave packet to reach a sensor.

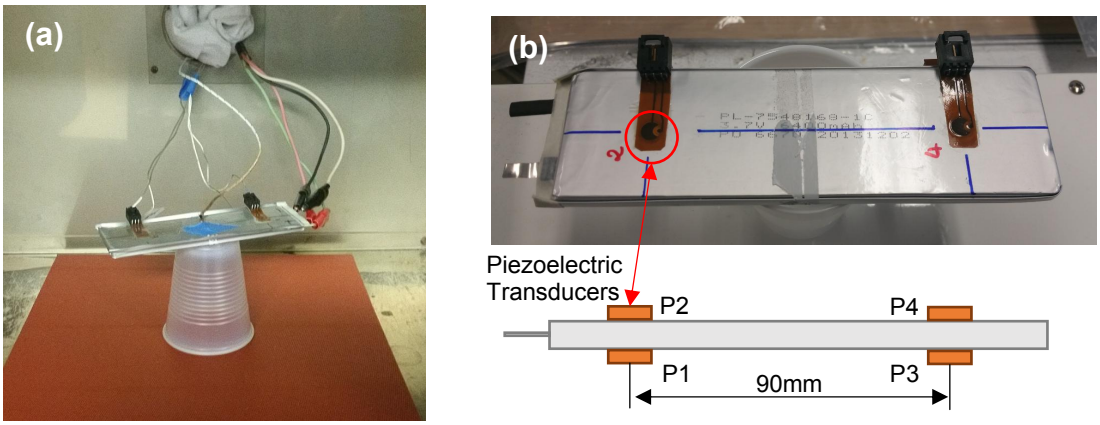

Figure 2 (a) Experimental setup used for electrical cycling and guided-wave data acquisition, in a low-temperature gravity-convection oven; (b) sensor locations on a 3650 mAh pouch battery, labeled P1 through P4.

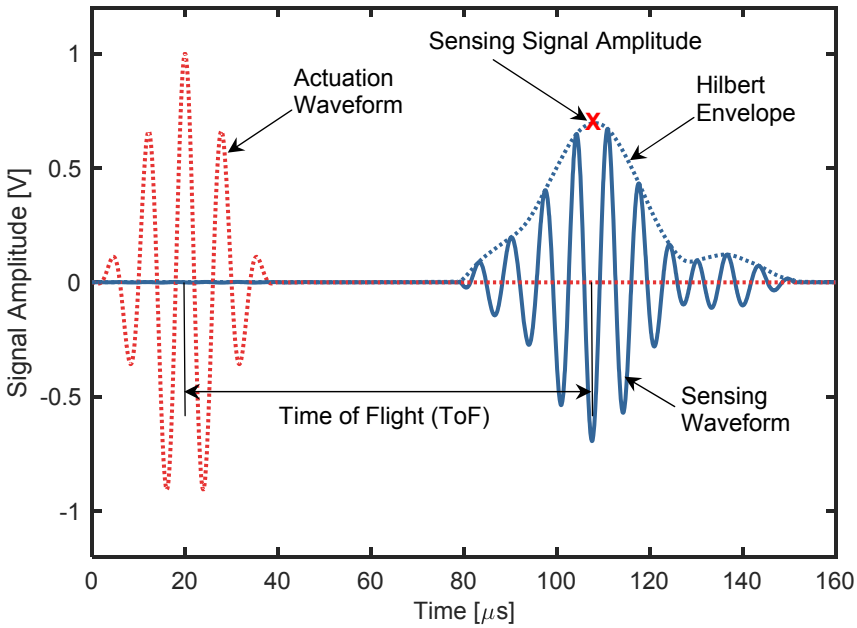

Figure 3 Representative signals from the P1-P3 transducer pair, using a tone-burst excitation at 125 kHz. The plot shows the definition of time of flight (ToF), which is the time taken for the actuation pulse to reach the sensor location; and signal amplitude which is the maximum amplitude of the sensing signal's Hilbert envelope.

4. RESULTS AND DISCUSSION

4.1 Variation in ToF and signal amplitude with SoC

The Li-ion batteries are cycled at a C/10 rate (a current rate at which the batteries would be fully charged in 10 hours), or equivalently 365 mA, at a constant temperature of 30 °C. As shown in Figure 4a, the cycle starts with charging at a constant current of 365 mAh (Region I) to a cutoff voltage of 4.2V. A 2-hour rest (Region II) is added before discharging at 365 mAh (Region III) to a cutoff voltage of 3.0V. The rest time between discharge and charge (not shown) is also set to 2 hours.

Guide-wave signal snapshots are analyzed over the period of the charge and discharge cycle, uncovering the behavior of the time-domain signal parameters with varying SoC. Figure 5 shows the receiving wave packet from a representative cell, at three instances in time during the charging phase (at three SoC levels (30%, 60%, and 90%), from the P1-P3 transducer pair, with a center frequency of 125 kHz. It can be seen that the wave packet moves faster, i.e. the ToF gets smaller, as SoC increases. At the same time, the signal amplitude of the receiving waves intensifies with increasing SoC.

Extracting and compositing the time-domain signal parameters in the same fashion at all SoC results in the behavior presented in Figure 4b, in comparison with the terminal voltage and applied current in Figure 4a. The ToF and signal amplitude are plotted against the elapsed time of the charge and discharge cycle. The ToF decreases monotonically during discharging, accounting for a net change of approximately 7μs, and vice versa for the discharge process. The increasing wave speed as the battery is charged implies changes in the composite medium's mechanical properties, most probably increasing modulus and/or declining stiffness [17]. This finding is in agreement with results from literature showing decrease in graphite anode's [18] and cathode's [19] densities, and increase in graphite's modulus [20] during charging. The NMC cathode however is reported to take on a lower modulus value with increasing cell SoC [21]; however, the absolute change of the cathode's modulus is much smaller than that of the anode.

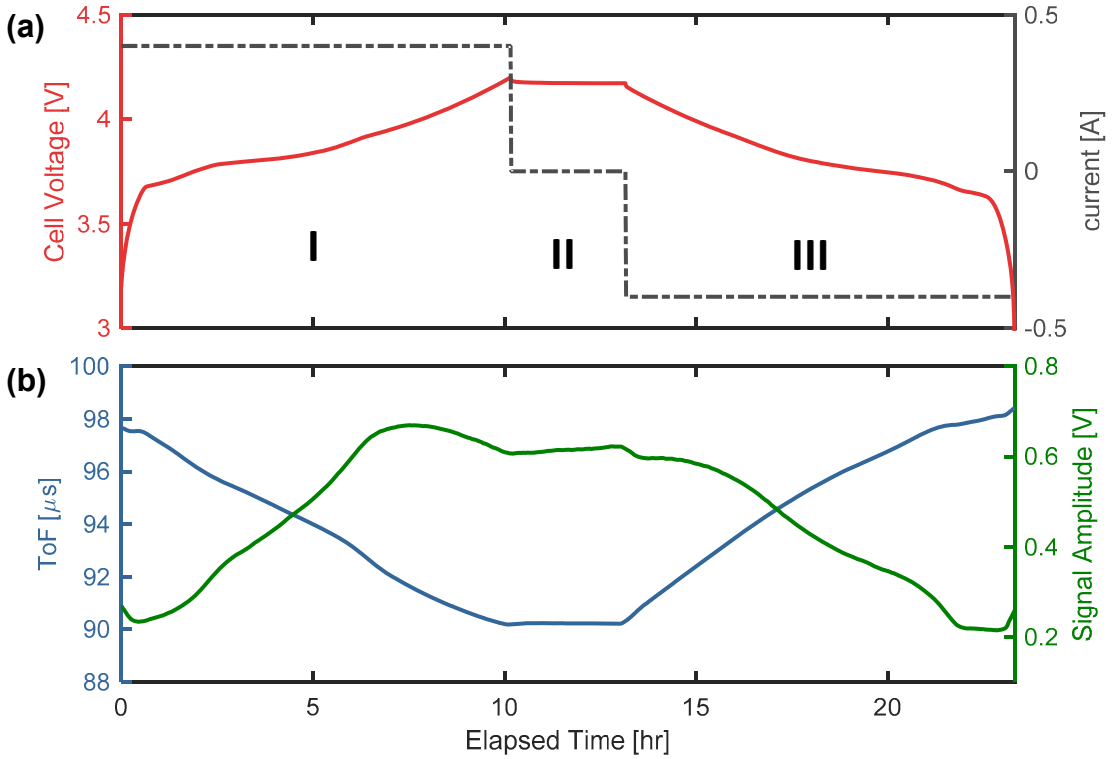

Figure 4 (a) Voltage and current data during a C/10 charging and discharging cycle, showing the charging phase (Region 1), rest period (Region II), and discharging phase (Region III); (b) Corresponding evolution of ToF and signal amplitude data taken every 1 minute (from P1-P3 transducer pair at 125 kHz).

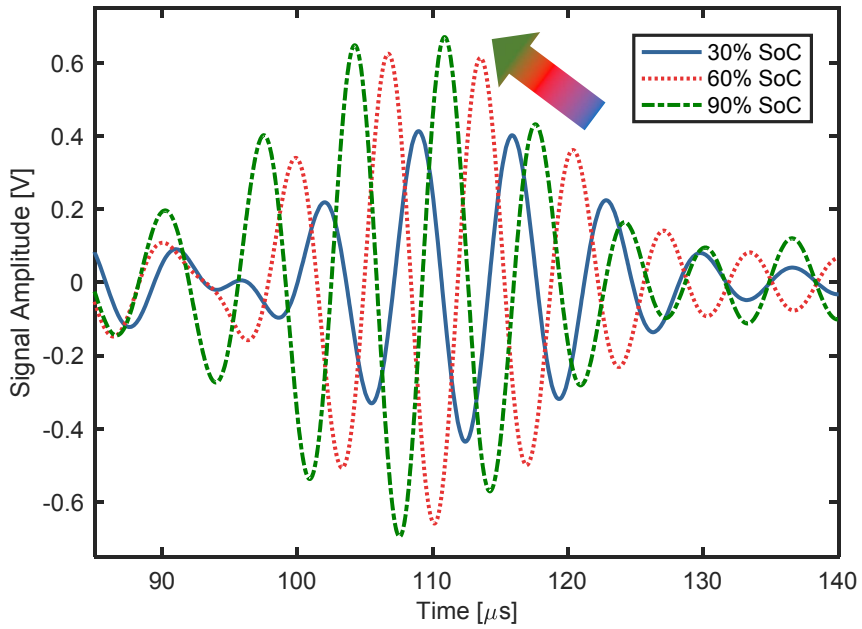

Figure 5 Influence of SoC on the guided-wave sensing signal during charging, showing increase in signal amplitude and shorter ToF with increasing SoC (from P1-P3 transducer pair at 125 kHz).

As seen in Figure 4b, the signal amplitude, on the other hand, increases with SoC for the majority of the charging process (terminal voltage between 3.7 and 3.95 V), except at the very beginning and at the end of charging. As the charge current is removed during the rest step, the signal amplitude relaxes slightly to an equilibrium level. Discharging is associated with minor fluctuation in signal amplitude at the beginning, then sees a monotonic decrease mostly through the rest of the process. The signal amplitude then increases sharply at the very end of discharging (terminal voltage < 3.6 V). While the ToF of the electrode composite can be calculated reasonably accurately through a numerical model, which is currently under investigation, the interpretation of signal attenuation's behavior is not straightforward as the propagation involves anisotropy, porosity, multiple phases, and interfaces.

In essence, it is evident that there is a strong correlation between the signal features of ultrasonic guided waves and the battery SoC, making guided-waves a viable technique for SoC estimation. Changes in the SoC are reflected in the changes in the density and elastic modulus of the anode and cathode materials, which in turn affect the behavior of the guided waves. Moreover, variations in the slopes of the signal amplitude and ToF versus time are seen at different instances throughout the charge and discharge processes. Besides the effect from the cathode phase transition, these non-linearities are primarily induced by the intercalation staging in the graphitic anode, as will be discussed in the following section.

4.2 Differential ToF revealing phase transitions

As observed in Figure 4b, although discernable, the sharp non-linear features are not well pronounced in the measured cell voltage curve. Using the voltage differential technique [22-24], the first derivative of the voltage, with respect to SoC during charging and depth of discharge (DoD) during discharging, dV/dQ, is calculated to clearly identify the underlying phases. The first derivative of the ToF with respect to SoC and DoD (dToF/dQ) could be calculated similarly to illustrate the phase-transition features in the ToF data.

Figures 5 shows dV/dQ and dToF/dQ with respect to SoC and DoD, during charging and discharging respectively. Pertaining to the nature of the NMC cathode, the global concave feature can be recognized in the calculated dV/dQ with respect to the SoC [25]. The local dV/dQ peaks can be associated with the stages of the graphite anode as it undergoes charging and discharging. The peaks are labeled 1, 2, 3, and 4 with increasing SoC levels (around 17%, 23%, 26%, and 60% SoC, respectively), and in reverse with increasing DoD. These peaks in dV/dQ coincide exactly with the sharp activities in the calculated dToF/dQ. Two additional troughs have been identified in dToF/dQ, although not evident in dV/dQ, at approximately 33% and 42% SoC, which are also believed to be ascribed to graphite staging.

More experiments, such as cyclic voltammetry, are being conducted to confirm the presence of the transition stages and correlating the features in guided-wave signals. Additionally, as phase transitioning occurs in a cell, it is hypothesized that changes in electrode's moduli and densities are simultaneously enhanced resulting in the peaks in dToF/dQ. To our best knowledge, even though changes in electrodes' moduli and densities with SoC are well documented in the literature [18-21], only their global behavior has been observed. Therefore, the differential ToF can potentially offer a new technique for accurately probing the transitioning behavior of battery's mechanics during charging and discharging.

It is also worth noting that the symmetry that is exhibited in dV/dQ during charging versus discharging is not shown in dToF/dQ. While discharging approximately reverses charging potential-wise, differences between charging and discharging are demonstrated through guided-wave signals. Most likely, removal and insertion of lithium from the graphite anode to the NMC cathode during discharging result in different characteristics of modulus and density distribution, as compared to the inverse charging process. This phenomenon is similar to one cathode behavior described by Wu et al. showing the variation in modulus and anisotropy in the metal oxide lattice due to different bond strengths during lithium intercalation and de-intercalation [21].

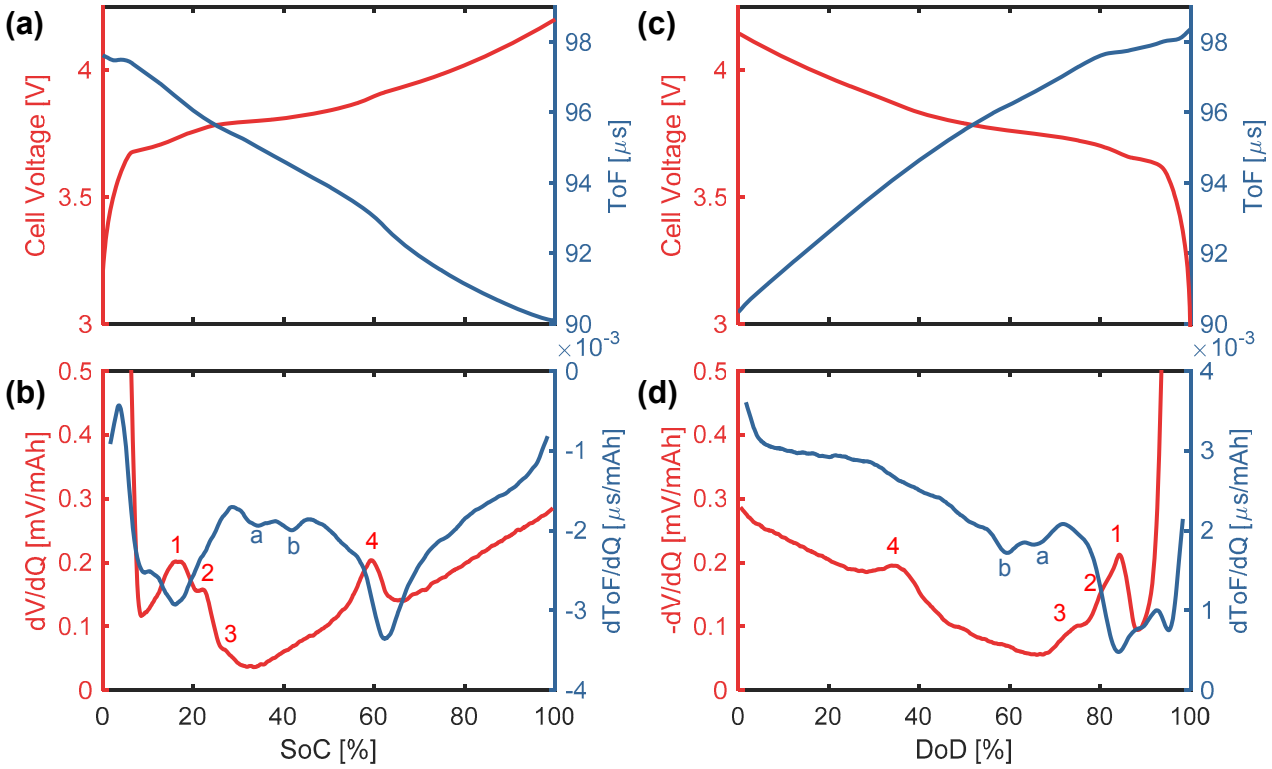

Figure 6 (a and c) Voltage and ToF data for a C/10 cycle during charging and discharging, respectively; (b and d) Corresponding first derivative of voltage and ToF with respect to capacity (dV/dQ and dToF/dQ) during charging and discharging, respectively. Negative values of dV/dQ are plotted in (d) to represent discharging. Guided-wave signals are from P1-P3 transducer pair, at 125 kHz.

4.3 Impact of cell aging

Following the charge-state analysis, an accelerated aging experiment is performed by aggressively charging and discharging the batteries to evaluate the impact of cell degradation on guided-wave signals. The cells are cycled at an elevated temperature of 45 °C with a more aggressive current rate of 3000 mA (0.8C) between 3.0 V and 4.2 V. A constant-voltage (CV) step is added after the cells have been charged to the maximum cutoff voltage, until the current drops to a cutoff value of 182.5 mA (C/20). The rest time before the discharge step is set to 15 minutes, with no rest period after discharging before the next charge step. A total of 200 charge and discharge cycles are performed.

The evolution of the signal parameters with increasing cycle number is shown in Figure 7b and 7c, respectively, while the terminal voltage profile is plotted in Figure 7a. An interesting behavior was observed in the cyclic ToF and signal amplitude as the battery ages. The ToF appears to globally shift towards a lower value, i.e. the wave speed is slower, with increasing cycle number. It should be noted that the shift in ToF due to aging is more prominent close to the end of discharge and the beginning of charge. It can also be seen that during charging and discharging, unlike in the rest period, the decrease rate of ToF with cycle number is not constant at a specific elapsed time (approximately the same SoC); i.e. the decline in ToF is more dramatic during the first 100 cycles than the latter half. On the other hand, as the cycle count increases, the signal amplitude gradually intensifies at all SoC levels. The amplification in the signal amplitude is less dramatic at the end of discharge and beginning of charge than elsewhere. Unlike ToF behavior, at a given SoC the rate at which the signal amplitude increases with respect to the cycle count is approximately constant with the cycle number.

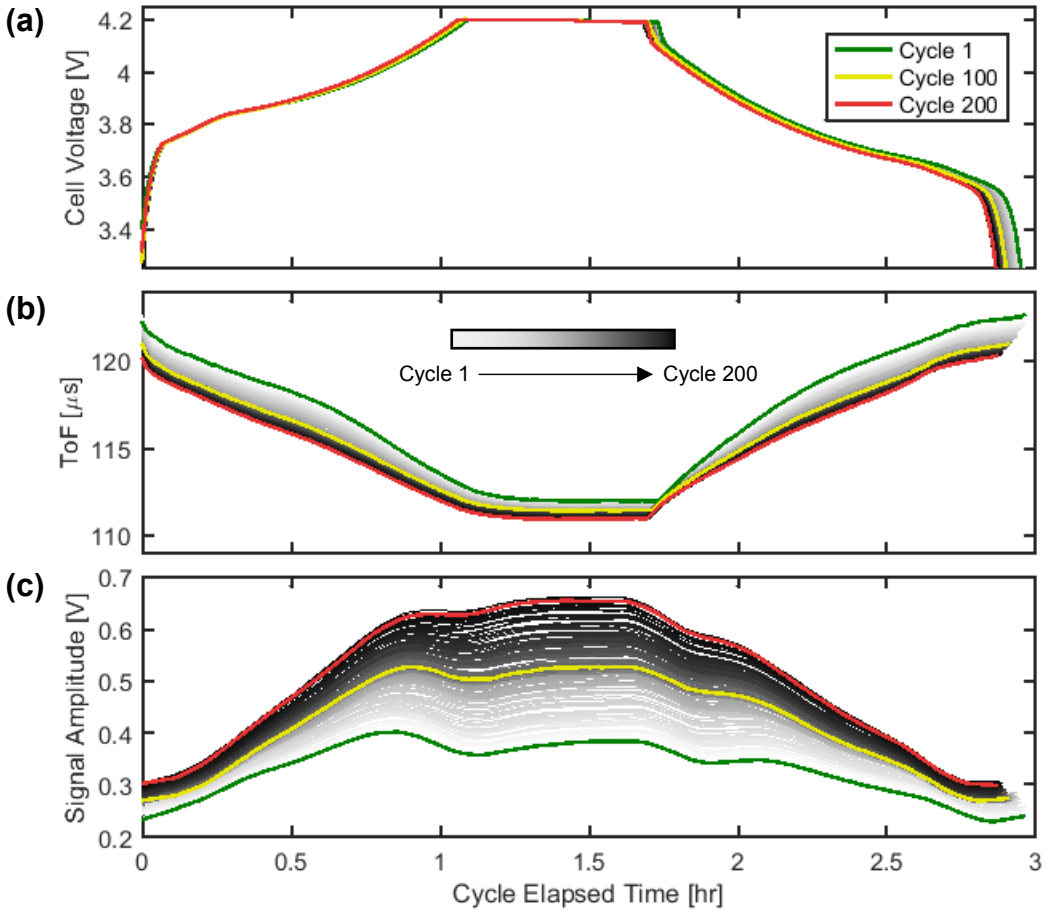

Figure 7 Cycle-to-cycle evolution of (a) terminal voltage, (b) ToF, and (c) signal amplitude, due to electrochemical aging shown in progressive shades of gray as a function of cycle elapsed time. Data from the first cycle is indicated in green, the 100th cycle indicated in yellow, and the 200th cycle indicated in red. Guided-wave signals are from P1-P3 transducer pair at 125 kHz.

The change in ToF and signal amplitude can be ascribed to the changes in mechanical properties (i.e. moduli and densities) due to battery degradation [26]. Lower ToF and higher signal amplitude suggest that aging might increase the battery's overall stiffness and/or lower the density. The underlying current- and SoC-dependent phenomena are also still under further investigation. As pointed out by Hsieh et al. [16], the scarcity and excess of lithium ions near the end of charge or discharge could also cause the abrupt stiffness change. The non-uniformity and rate-dependence are otherwise relaxed during the rest step.

So as to filter out the rate and SoC effects, the ToF and signal amplitude at the end of the rest step for every cycle are extracted and shown in Figure 8b. The remaining capacity with respect to the cycle number is plotted in Figure 8a for comparison. An obvious correlation between the guided-wave signal parameters and the cycle count, and thus capacity fading, can be observed. As the battery ages, the ToF, at a fully-charged relaxed state, declines, while the signal amplitude increases, though not linearly with cycle count. This finding can be potentially very useful for developing a technique for the determination of SoH and remaining useful life. In service, when the batteries are fully-charged and at rest (e.g. a fully-charged electric vehicle at idle), they can be probed for the guided-wave ToF and amplitude. The SoH can be estimated by comparing the current signal parameters with the values from a look-up table (similar to Figure 7b) pre-collected from a set of baseline cells; or even predicted for a number of cycles ahead. Such guided-wave-based SoH estimation models are currently being developed and will be discussed in detail in a future paper.

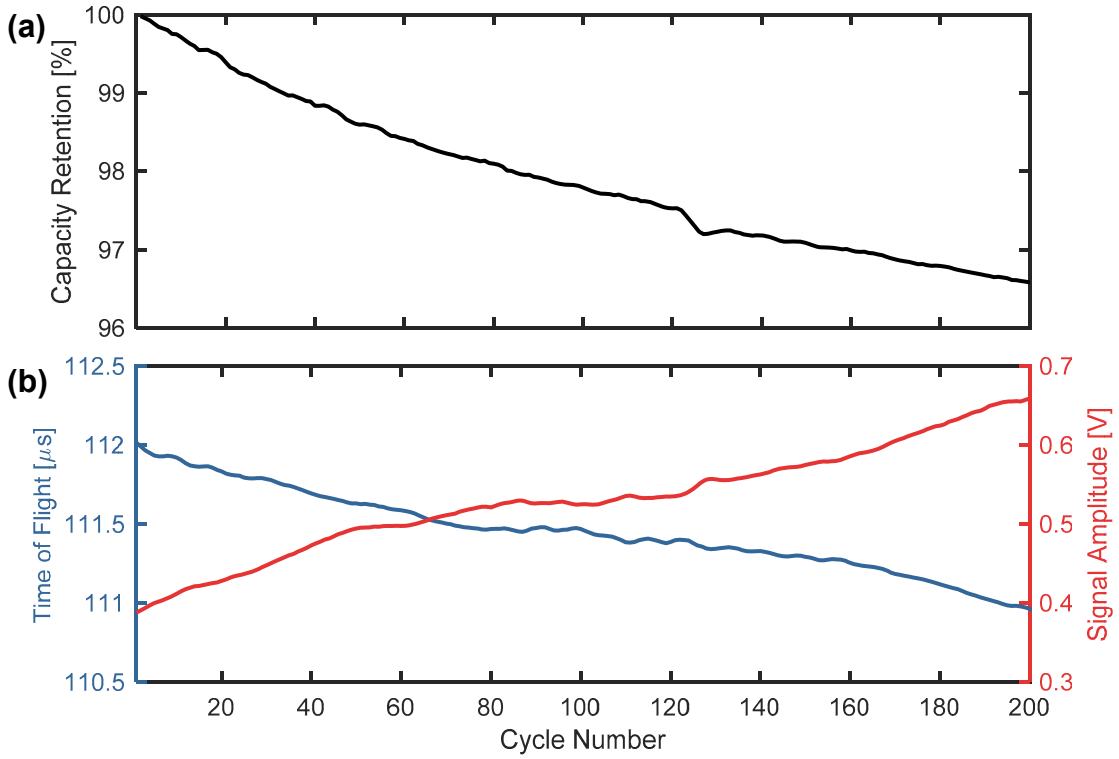

Figure 8 (a) Capacity retention (normalized by the first-cycle capacity) as a function of the cycle number; (b) correlation between cycle number and guided-wave signal amplitude and ToF at the end of rest period after charging, showing monotonic increase in signal amplitude and decrease in ToF with capacity fade. Guided-wave signals are from P1-P3 transducer pair at 125 kHz.

4.4 Analysis of aging mechanisms through differential ToF

The causes and mechanisms of capacity fading in Li-ion batteries can be very complex, involving side reactions, irreversible loss of active materials, etc. The differential voltage analysis has been shown to effectively probe the degradation mechanisms in Li-ion batteries and uncover the degradation process in the life of a battery [27, 28]. Similarly, through a differential ToF analysis, the shifts in the derivative of the guided-wave signal features can potentially be used to help pinpoint the underlying degradation process.

The first derivative of the terminal voltage, dV/dQ, is calculated for the C/10 cycle (at 30 °C) of a fresh cell and after the aforementioned 200-cycle aging, as shown in Figures 9a and 9c, for charging and discharging respectively. As a comparison, dToF/dQ before and after aging is plotted in Figures 9b and 9d, respectively. The most pronounced activity is the shift of the dV/dQ peaks labeled 1 through 4 towards a higher SoC as the cell ages, accompanied by dramatic activities in dToF/dQ at the same capacity levels. The dToF/dQ analysis also reveals two additional troughs due to degradation during charging, labeled c' and d' near the end of charge, which are otherwise not evident in dV/dQ. It is also noted that apart from a subtle change in the concavity of dV/dQ and dToF/dQ, the relative distance between the peaks and troughs remain the same, as can be clearly observed from the gap between the peaks 1 and 4.

It can be concluded that the degradation mechanisms that cause the changes observed in dV/dQ are fundamentally mechanical phenomena, i.e. changes in moduli and densities, because similar activities are also demonstrated in guided-wave dToF/dQ. The fact that the relative peak-to-peak distances remain intact suggests that there is minimal loss the active negative electrode (graphite) material, i.e. the number of active sites in graphite, for lithium intercalation, remains constant [27]. The shift of dV/dQ and dToF/dQ is therefore ascribed to the irreversible loss of lithium ions, most probably due to the solid electrolyte interface (SEI) layer formation on the graphitic electrode [27]. The slight change in the

concavity might also be associated with the positive material (NMC cathode) loss [29], but will be confirmed through detailed characterization using half cells in future work. Nonetheless, the degradation phenomena inferred from the differential ToF are remarkably in line with those reported in literature for high-temperature cycling of graphite/NMC Li-ion batteries, demonstrating aging that is lithium loss limiting accompanied by moderate cathode capacity loss [29, 30].

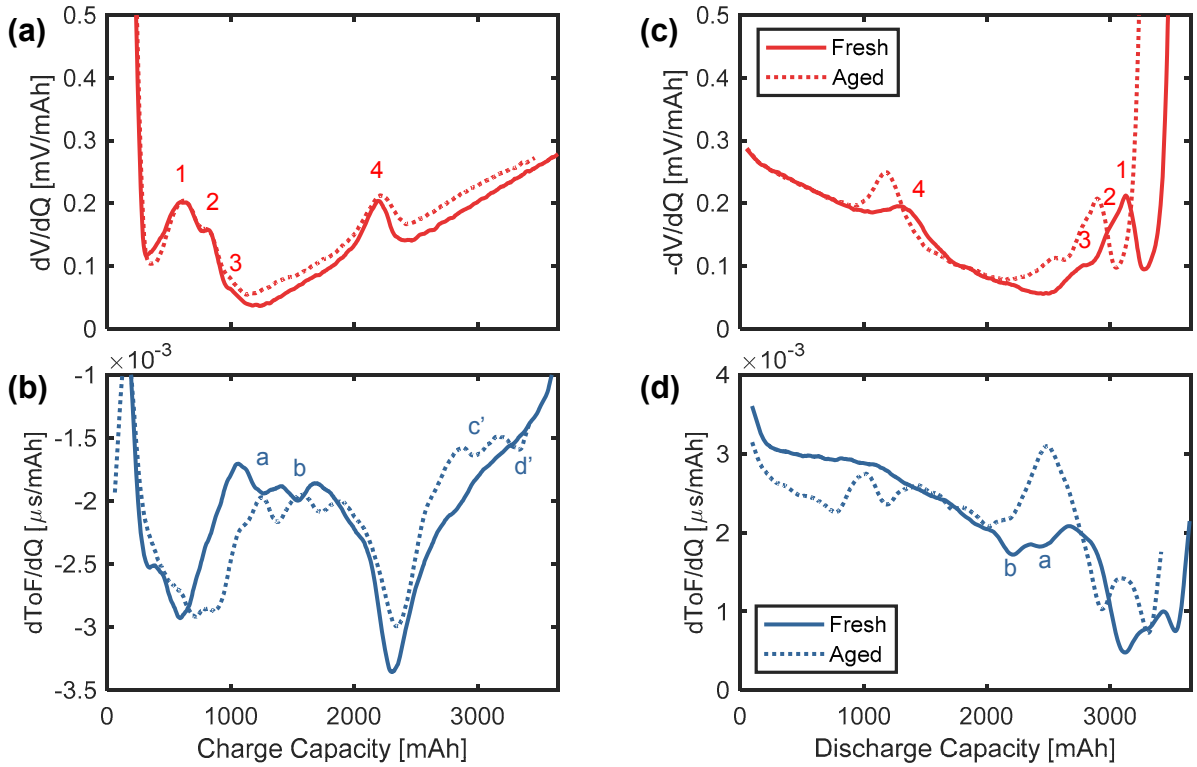

Figure 9 Impact of aging on differential voltage and ToF. (a and c) dV/dQ with respect to charge and discharge capacity, during charging and discharging, respectively. Data from a fresh cell is indicated in solid line, post-cycled data indicated in dotted line; (b and d) corresponding dToF/dQ. Guided-wave signals are from P1-P3 transducer pair at 125 kHz.

5. CONCLUSIONS

This work demonstrated the feasibility of using ultrasonic guided waves, with small-footprint surface-mounted piezoelectric transducers for probing lithium-ion battery's states during charging and discharging, as well as cycle life aging. Pitch-catch guided-wave signal parameters were obtained from built-in piezo-transducers on lithium-ion batteries during cycling and aging processes. The obtained results suggest that this technique can potentially become an effective real-time in-service method for accurately estimating SoC and SoH. In essence, it has been shown herein through our preliminary findings that:

- The time domain analysis of guided-wave signal parameters, namely ToF and signal amplitude, provides a strong repeatable correlation with battery's SoC, hence possibly offering a new method for non-electrical-contact SoC estimation.
- The evolution of cyclic ToF and signal amplitude as a result from capacity fade infers the mechanical nature of battery degradation. Complimentary to the traditional voltage-based measurement, guided-wave signals deliver an additional piece of information, necessary for directly determining SoH.

- The differential ToF analysis is shown to be able to uncover the phase transition behavior, coinciding with enhanced distribution and redistribution of electrodes' mechanical properties during charging and discharging. Tracing the evolution of dToF/dQ due to aging can offer a new non-invasive in-situ technique for determining the root cause of cycle life deterioration.
- Guided-wave analysis nonetheless can potentially assist scientists in providing fundamental insights on structural and mechanical activities inside a battery, such as moduli, porosity, and densities, beyond conventional electrochemical methods.

More detailed investigation is underway for correlating signal parameters with physical phenomena of a battery undergoing charging and discharging along with the aid of numerical modelling. Last but not least, the results presented heretofore will be used to assist in establishing a guided-wave-based model for real-time SoC and SoH prediction. As with guided-wave-based structural health monitoring (SHM), the concept can also be extended and applied to structural energy storage, a concept newly introduced in literature [31-33], for simultaneous structural and battery state monitoring.

ACKNOWLEDGEMENTS

The work is supported by the Advanced Research Projects Agency - Energy (U.S. Department of Energy) through the ARPA-E Award No. DE-AR0000393. The authors highly appreciate support from Dr. Keith Kepler, Dr. Hongjian Liu, and Dr. Michael Slater at Farasis Energy Inc. for valuable feedback and suggestions.

REFERENCES

[1] Goodenough, J. B., and Park, K.-S., "The Li-Ion Rechargeable Battery: A Perspective," Journal of the American Chemical Society, 135(4), 1167-1176 (2013).

[2] Liu, P., Ross, R., and Newman, A., "Long-range, low-cost electric vehicles enabled by robust energy storage," MRS Energy & Sustainability, 2, E12 (2015).

[3] Lu, L., Han, X., Li, J., Hua, J., and Ouyang, M., "A review on the key issues for lithium-ion battery management in electric vehicles," Journal of Power Sources, 226, 272-288 (2013).

[4] Etacheri, V., Marom, R., Elazari, R., Salitra, G., and Aurbach, D., "Challenges in the development of advanced Li-ion batteries: a review," Energy & Environmental Science, 4(9), 3243-3262 (2011).

[5] Waag, W., Fleischer, C., and Sauer, D. U., "Critical review of the methods for monitoring of lithium-ion batteries in electric and hybrid vehicles," Journal of Power Sources, 258, 321-339 (2014).

[6] Zhang, J., and Lee, J., "A review on prognostics and health monitoring of Li-ion battery," Journal of Power Sources, 196(15), 6007-6014 (2011).

[7] Lu, Z., and Dahn, J. R., "Understanding the anomalous capacity of Li/Li [Ni x Li (1/3− 2x/3) Mn (2/3− x/3)] O 2 cells using in situ X-ray diffraction and electrochemical studies," Journal of The Electrochemical Society, 149(7), A815-A822 (2002).

[8] Wang, X.-J., Chen, H.-Y., Yu, X., Wu, L., Nam, K.-W., Bai, J., Li, H., Huang, X., and Yang, X.-Q., "A new in situ synchrotron X-ray diffraction technique to study the chemical delithiation of LiFePO 4," Chemical Communications, 47(25), 7170-7172 (2011).

[9] Nam, K. W., Bak, S. M., Hu, E., Yu, X., Zhou, Y., Wang, X., Wu, L., Zhu, Y., Chung, K. Y., and Yang, X. Q., "Combining In Situ Synchrotron X□Ray Diffraction and Absorption Techniques with Transmission Electron Microscopy to Study the Origin of Thermal Instability in Overcharged Cathode Materials for Lithium□Ion Batteries," Advanced Functional Materials, 23(8), 1047-1063 (2013).

[10] Sharma, N., Peterson, V. K., Elcombe, M. M., Avdeev, M., Studer, A. J., Blagojevic, N., Yusoff, R., and Kamarulzaman, N., "Structural changes in a commercial lithium-ion battery during electrochemical cycling: An in situ neutron diffraction study," Journal of Power Sources, 195(24), 8258-8266 (2010).

[11] Wang, X.-L., An, K., Cai, L., Feng, Z., Nagler, S. E., Daniel, C., Rhodes, K. J., Stoica, A. D., Skorpenske, H. D., Liang, C., Zhang, W., Kim, J., Qi, Y., and Harris, S. J., "Visualizing the chemistry and structure dynamics in lithium-ion batteries by in-situ neutron diffraction," Scientific Reports, 2, 747 (2012).

[12] Tröltzsch, U., Kanoun, O., and Tränkler, H.-R., "Characterizing aging effects of lithium ion batteries by impedance spectroscopy," Electrochimica Acta, 51(8–9), 1664-1672 (2006).

[13] Waag, W., Käbitz, S., and Sauer, D. U., "Experimental investigation of the lithium-ion battery impedance characteristic at various conditions and aging states and its influence on the application," Applied Energy, 102, 885-897 (2013).
[14] Sood, B., Osterman, M., and Pecht, M., "Health monitoring of lithium-ion batteries." 1-6.
[15] Gold, L., Bach, T., Virsik, W., Schmitt, A., Müller, J., Staab, T. E., and Sextl, G., "Probing lithium-ion batteries' state-of-charge using ultrasonic transmission–Concept and laboratory testing," Journal of Power Sources, 343, 536-544 (2017).
[16] Hsieh, A., Bhadra, S., Hertzberg, B., Gjeltema, P., Goy, A., Fleischer, J., and Steingart, D., "Electrochemical-acoustic time of flight: in operando correlation of physical dynamics with battery charge and health," Energy & environmental science, 8(5), 1569-1577 (2015).
[17] Giurgiutiu, V., [Structural health monitoring: with piezoelectric wafer active sensors] Academic Press, (2007).
[18] Koyama, Y., Chin, T. E., Rhyner, U., Holman, R. K., Hall, S. R., and Chiang, Y. M., "Harnessing the Actuation Potential of Solid□State Intercalation Compounds," Advanced Functional Materials, 16(4), 492-498 (2006).
[19] Reimers, J. N., and Dahn, J. R., "Electrochemical and In Situ X□Ray Diffraction Studies of Lithium Intercalation in Li x CoO2," Journal of The Electrochemical Society, 139(8), 2091-2097 (1992).
[20] Qi, Y., Guo, H., Hector, L. G., and Timmons, A., "Threefold increase in the Young's modulus of graphite negative electrode during lithium intercalation," Journal of The Electrochemical Society, 157(5), A558-A566 (2010).
[21] Wu, L., and Zhang, J., "Ab initio study of anisotropic mechanical properties of LiCoO2 during lithium intercalation and deintercalation process," Journal of Applied Physics, 118(22), 225101 (2015).
[22] Bloom, I., Jansen, A. N., Abraham, D. P., Knuth, J., Jones, S. A., Battaglia, V. S., and Henriksen, G. L., "Differential voltage analyses of high-power, lithium-ion cells: 1. Technique and application," Journal of Power Sources, 139(1), 295-303 (2005).
[23] Dahn, H. M., Smith, A., Burns, J., Stevens, D., and Dahn, J., "User-friendly differential voltage analysis freeware for the analysis of degradation mechanisms in Li-ion batteries," Journal of The Electrochemical Society, 159(9), A1405-A1409 (2012).
[24] Zhang, Y., Wang, C.-Y., and Tang, X., "Cycling degradation of an automotive LiFePO 4 lithium-ion battery," Journal of Power Sources, 196(3), 1513-1520 (2011).
[25] Bloom, I., Walker, L. K., Basco, J. K., Abraham, D. P., Christophersen, J. P., and Ho, C. D., "Differential voltage analyses of high-power lithium-ion cells. 4. Cells containing NMC," Journal of Power Sources, 195(3), 877-882 (2010).
[26] Cannarella, J., and Arnold, C. B., "Stress evolution and capacity fade in constrained lithium-ion pouch cells," Journal of Power Sources, 245, 745-751 (2014).
[27] Deshpande, R., Verbrugge, M., Cheng, Y.-T., Wang, J., and Liu, P., "Battery cycle life prediction with coupled chemical degradation and fatigue mechanics," Journal of the Electrochemical Society, 159(10), A1730-A1738 (2012).
[28] Smith, A. J., Dahn, H. M., Burns, J. C., and Dahn, J. R., "Long-Term Low-Rate Cycling of LiCoO2/Graphite Li-Ion Cells at 55°C," Journal of The Electrochemical Society, 159(6), A705-A710 (2012).
[29] Jalkanen, K., Karppinen, J., Skogström, L., Laurila, T., Nisula, M., and Vuorilehto, K., "Cycle aging of commercial NMC/graphite pouch cells at different temperatures," Applied Energy, 154, 160-172 (2015).
[30] Wang, J., Purewal, J., Liu, P., Hicks-Garner, J., Soukazian, S., Sherman, E., Sorenson, A., Vu, L., Tataria, H., and Verbrugge, M. W., "Degradation of lithium ion batteries employing graphite negatives and nickel–cobalt–manganese oxide + spinel manganese oxide positives: Part 1, aging mechanisms and life estimation," Journal of Power Sources, 269, 937-948 (2014).
[31] Ladpli, P., Nardari, R., Kopsaftopoulos, F., Wang, Y., and Chang, F.-K., "Design of Multifunctional Structural Batteries with Health Monitoring Capabilities," European Workshop on Structural Health Monitoring, (2016).
[32] Ladpli, P., Nardari, R., Rewari, R., Liu, H., Slater, M., Kepler, K., Wang, Y., Kopsaftopoulos, F., and Chang, F.-K., "Multifunctional Energy Storage Composites: Design, Fabrication, and Experimental Characterization," ASME Power & Energy, V002T01A004-V002T01A004 (2016).
[33] Ladpli, P., Nardari, R., Wang, Y., Hernandez-Gallegos, P. A., Rewari, R., Kuo, H. T., Kopsaftopoulos, F., Kepler, K. D., Lopez, H. A., and Chang, F., "Multifunctional Energy Storage Composites for SHM Distributed Sensor Networks," International Workshop on Structural Health Monitoring, (2015).